Noise estimation in infrared image sequences: a tool for the quantitative evaluation of the effectiveness of registration algorithms

(Article begins on next page)

17 April 2024

Valentina Agostini[1], Silvia Delsanto[1], Marco Knaflitz[1], *Member, IEEE* and Filippo Molinari[1], *Member,*

IEEE

[1]Dip. Elettronica, Politecnico di Torino, Corso Duca degli Abruzzi 24, 10129 Torino, Italy

Noise estimation in infrared image sequences: a tool for the quantitative evaluation of the effectiveness of registration algorithms

Abstract — Dynamic infrared imaging has been proposed in literature as an adjunctive technique to mammography in breast cancer diagnosis. It is based on the acquisition of hundreds of consecutive thermal images with a frame rate ranging from 50 frames/s to 200 frames/s, followed by the harmonic analysis of temperature time series at each image pixel. However, the temperature fluctuation due to blood perfusion, which is the signal of interest, is small compared to the signal fluctuation due to subject movements. Hence, before extracting the time series describing temperature fluctuations, it is fundamental to realign the thermal images to attenuate motion artifacts. In this paper, we describe a method for the quantitative evaluation of any kind of feature-based registration algorithm on thermal image sequences, provided that an estimation of local velocities of reference points on the skin is available. As an example of evaluation of a registration algorithm, we report the evaluation of the signal to noise ratio improvement obtained by applying a non-rigid piecewise linear algorithm.

I. INTRODUCTION

Currently, the screening gold standard in breast cancer diagnosis is mammography. Since the early seventies, thermography has been proposed as a possible adjunct to mammography in screening, but static thermography - i.e., the simple measurement of breast skin temperature - yielded no satisfactory results [1]. More recently, Dynamic Area Telethermometry (DAT) [2-3], also known as Dynamic InfraRed Imaging (DIRI) [4-5], has been proposed as a new imaging modality for breast cancer detection. It requires the acquisition of a sequence of hundreds of consecutive thermal images with a rate ranging from 50 frames/s to 200 frames/s. The harmonic analysis of the time course of temperature fluctuations allows to obtain information on the local blood perfusion. In literature, it has been reported that temperature fluctuations have an important diagnostic value in oncology [2-3]. In fact, recent studies have demonstrated that cancer-associated extra vascular nitric oxide determines a perturbation in the normal modulation of the local blood flow, which can be detected through the analysis of the fluctuations of temperature at each sample region [2-5]. Hence, after subdividing the region of interest in square sub-regions (approximately 4 mm^2 each) consisting of one or more pixels, spectral analysis of the temperature time series corresponding to each sub-region is performed.

In our experimental protocol, the acquisition of the image sequence lasts 10 seconds, during which the patient's breast moves non-rigidly due to physiological (breathing, heart activity, …) and random movements. Consequently, the signal of interest, i.e., the small temperature fluctuations due to perturbations of the blood perfusion in a certain region, is superimposed to signal fluctuations arising from the subject motion. This is because temperature samples corresponding to different skin regions are recorded as belonging to the same region observed by the infrared sensor. Motion artifacts are then particularly relevant in areas in which a strong spatial gradient of temperature is present.

52 Therefore, before proceeding with the harmonic analysis of the temperature time series in each square

53 sub-region, it is fundamental to properly realign the thermal images composing the sequence to attenuate

54 motion artifacts. Although some Authors have reported the detrimental effect of motion artifacts [4], at

55 this time there is no quantitative evaluation of the power due to the effects of motion artifacts with respect

56 to that of the signal of interest. This also limits the possibility of objectively evaluating the performance

57 of different algorithms for realigning infrared sequences [6].

58 The goal of this paper is to propose a method to quantitatively evaluate the performances of marker-

59 based registration algorithms in dynamic infrared imaging, in terms of improvement of the signal to noise

60 ratio. This approach can be applied to any kind of registration algorithm based on control points, provided

61 that an estimation of local image velocities is available. We then present the results obtained by applying

62 the proposed approach to evaluate the improvement of the signal to noise ratio obtained through a

63 piecewise linear registration algorithm applied to sequences relative to three subjects with different breast

64 size.

65 II. MATERIALS AND METHODS

66 *A. The model*

67 First, we introduce a model for the noise estimation in dynamic infrared imaging. Considering a small

68 portion of skin and indicating by *T(x,y,t)* the temperature that the infrared sensor measures in the point

69 *(x,y)* at a given time instant *t*, temperature variations in time captured by the infrared camera are a

70 combination of the physiological variations of the skin temperature (the signal of interest) and of apparent

71 temperature changes actually due to patient's movements (noise).

72 The total derivative of temperature with respect to time, *dT/dt,* is:

73

74
$$\frac{dT}{dt} = \frac{\partial T}{\partial t} + \frac{\partial T}{\partial x}\frac{\partial x}{\partial t} + \frac{\partial T}{\partial y}\frac{\partial y}{\partial t} =$$
$$= \frac{\partial T}{\partial t} + (\vec{v}\cdot\nabla)T \qquad (1)$$

75 where $\frac{\vdash\!\!\!\dashv}{|\vdash\!\!\!\dashv|}(v_x, v_y)$ is the 2-dimensional velocity of the skin portion and ∇T is the spatial temperature

76 gradient. Equation 2 reports the expression of the noise $N(x,y,t)$ introduced by motion artifacts.

$$N(x,y,t) \approx \int_0^t \vec{v}(x,y,t') \cdot \nabla T(x,y,t')dt' \qquad (2)$$

78 A measure of the performance of a realignment algorithm applied to the infrared image sequence is the

79 improvement of the signal-to-noise ratio obtained through the registration. The signal-to-noise ratio of the

80 process - at each point *(x,y)* - is defined as $S/N \equiv \sigma_T^2(x,y)/\sigma_N^2(x,y)-1$, where $\sigma_T^2(x,y)$ is the

81 variance of the measured temperature time series *T(x,y,t)* (signal plus noise) and $\sigma_N^2(x,y)$ is the variance

82 of the noise, as given by Eq. (2). Similarly, we define the signal-to-noise ratio after registration as

83 $(S/N)_R \equiv \sigma_{T_R}^2(x,y)/\sigma_{N_R}^2(x,y)-1$, where $\sigma_{T_R}^2(x,y)$ is the variance of the measured temperature time

84 series *T_R(x,y,t)* obtained after sequence realignment and $\sigma_{N_R}^2(x,y)$ is the variance of the

85 term $\int_0^t \vec{v}_R(x,y,t') \cdot \nabla T_R(x,y,t')dt'$, being $\vec{v}_R(x,y,t)$ the residual velocity, not compensated by the

86 registration algorithm.

87 *B. Acquisition system and patient positioning*

88 The infrared image sequences were acquired with an AIM256Q camera (Long Wave Quantum Well

89 Infrared Photodetector, 256×256 pixels, produced by AEG Infrarot-Module GmbH, Germany). The

90 acquisition time was equal to 10 seconds and the frame rate was 50 frames/s; hence, each sequence

91 consisted of 500 thermal images of 256×256 pixels.

92 The sensor noise declared by the constructor of the infrared camera is equal to 17.3 mK (given as

93 NETD, with an integration time of 20 ms) and thus is negligible compared to noise due to patient's

94 movement, estimated by simulations, which is typically of the order of hundreds of mK. Hence, in our

95 model, we considered the patient's movement as the only noise source.

96 The patient was asked to lie down onto an examination table with a backrest inclination of 40 degrees

97 with respect to the horizontal plane. She was also asked to raise up her arms with the hands resting over

98 her head. We acquired a frontal view comprehending both breasts.

99 Before the acquisition, two sets of wooden spherical markers (5 mm in diameter) were applied to the

100 skin to obtain a) control points, i.e. contrasted features for registration, and b) test points, for evaluating

101 the goodness of the registration itself. In particular, as control points we placed 6-8 equally spaced

102 markers around each breast contour, one roughly at the center of the previous ones, and 2 on the sternum.

103 Test points consisted of markers applied internally to each breast contour. All markers were fixed to the

104 skin by means of biocompatible glue. Figure 1a shows a typical placement of control points (light-colored

105 markers) and of test points (dark markers).

106 III. IMAGE REGISTRATION AND REGISTRATION EVALUATION

107 *A. Image Registration*

108 The first step in any feature-based registration is the detection of the control points that are used to

109 compute the transformation. To localize control and test points, we developed a specific algorithm for the

110 automatic segmentation of the image and labeling of markers [6].

111 Centroids of control points were used to obtain a piece-wise linear transformation based on a Delaunay

112 triangulation [7] of the region to be registered. Figure 1b shows an example of triangulation. We chose

113 this specific transformation because it is reported to give good results when small geometric differences

114 between the images to be registered are expected [8], as in this case.

115 Here we reported the specific registration algorithm we adopted only for the sake of completeness, but

116 we emphasize that the signal-to-noise ratio estimation method we propose can be applied to any kind of

117 registration algorithm based on control points, if an estimation of local image velocities is available.

118 *B. Registration Evaluation*

119 In order to evaluate the signal-to-noise ratio before and after the registration, we estimated the velocities

120 $\vec{v}$ and $\vec{v}_R$. We tested, on the three subjects that were included in this paper, different algorithms to

121 interpolate the velocities, both in the registered and in the non-registered sequences. We benchmarked the

122 results using Nearest-Neighbors (NN), Linear Interpolation (LI), and Biharmonic Spline Interpolation

123 (SI), for estimating the velocities within the region of interest. Results, in terms of SNR quantification,

124 were different from subject to subject: for subject 1 (small breast size) LI was better than the others, for

125 subject 3 (large breast size) NN was the best, and for subject 2 (medium breast size) all the techniques

126 behaved similarly. Specifically, considering the three interpolation techniques applied to subject 2

127 (medium breast size) in terms of SNR increment due to registration no statistical significance was found

128 (Student's t-test, $P > 0.05$). Presently, our results do not show any significant difference among the

129 techniques we tested. We chose NN since we believe it gives acceptable results in most of the tested

130 conditions and for the majority of the subjects (medium breast size). To this purpose, we calculated the

131 Voronoi regions [9] associated to test marker centroids (see Fig. 1c) and assumed that the points

132 belonging to the same Voronoi region had equal velocity.

133 The instantaneous velocity $\vec{v}$ of a certain marker centroid (x_t, y_t) at time t was calculated using a two-

134 point forward approximation:

135
$$v_{x,t} = \frac{x_{t+1} - x_t}{\Delta t} \; ; \; v_{y,t} = \frac{y_{t+1} - y_t}{\Delta t} \; ,$$

136 where $\Delta t = 20$ ms is the sampling period.

137 The image gradient is computed using the digital approximation of the first order derivative in its anti-

138 symmetrical and linear implementation, i.e. by convolving the image with the vector [-0.5 0 0.5]).

IV. UNCERTAINTY IN SNR CALCULATION

140 The SNR depends on velocities and temperature gradients as stated by Eq. 2. In this Section we show

141 how the localization error affects the SNR estimation and we provide a worst-case estimate of the

142 uncertainty.

143 The uncertainty on the SNR may be expressed by the uncertainty on the noise computed according to

144 Eq. 2, in which $\vec{v}$ and ∇T are independent variables. Let *u(x)* end *u(y)* be respectively the uncertainty

145 on the localization of marker centroids along x and y. The uncertainty on the noise value is expressed by

146 Eq. 3.

147 $$u(N(x,y,t)) = \sqrt{\left(\frac{\partial \int_0^t \vec{v}(x,y,t') \cdot \nabla T(x,y,t')dt'}{\partial x} u(x)\right)^2 + \left(\frac{\partial \int_0^t \vec{v}(x,y,t') \cdot \nabla T(x,y,t')dt'}{\partial y} u(y)\right)^2} \quad (3)$$

148 By applying the partial derivative operator on the first term of Eq. 3 we obtain Eq. 4, in which, by

149 assuming the tissue as locally inextensible ($\frac{\partial \vec{v}(x,y,t')}{\partial x} = 0$), we can neglect the first term.

150 $$\frac{\partial \int_0^t \vec{v}(x,y,t') \cdot \nabla T(x,y,t')dt'}{\partial x} = \int_0^t \left[\frac{\partial \vec{v}(x,y,t')}{\partial x} \cdot \nabla T(x,y,t') + \vec{v}(x,y,t') \cdot \frac{\partial \nabla T(x,y,t')}{\partial x}\right]dt' \quad (4)$$

151 The second term of Eq. 3 may be treated similarly. Assuming that the behavior along x and y is similar,

152 the two terms of Eq. 3 may be considered as equal. It follows that

153 $$u(N(x,y,t)) = \sqrt{2 \cdot \left[\int_0^t \vec{v} \cdot \frac{\partial \nabla T}{\partial x}dt'\right]^2 \cdot [u(x)]^2} \cong \sqrt{2 \cdot \left[\frac{\Delta x}{\Delta t} \cdot \frac{\partial \nabla T}{\partial x} \cdot \Delta t\right]^2 \cdot [u(x)]^2} \quad (5)$$

154 Posing $\Delta x = 0.1\,\text{px}$, $\frac{\partial \nabla T}{\partial x} = 0.25\,\text{K·px}^{-2}$, $u(x) = 0.015\,\text{px}$ (values obtained from our database of images

155 using a 8-time oversampling [6]), we obtain a value of noise uncertainty of the order of 0.5 mK. After

156 realignment with a piecewise linear algorithm we have a residual error approximately equal to 20 mK,

157 and hence forty times larger than noise uncertainty. Hence, the uncertainty on the SNR value is

158 approximately 0.25 dB.

159 In order to test the dependence of the proposed SNR measure on the accuracy of the calculated

160 velocities we performed a robustness analysis considering different registration transformations:

161 PieceWise Linear (PWL), Polynomial of order 4 (P4), and Linear Conformal (LC), i.e., a transformation

162 that can include a rigid roto-translation, and/or a scaling. The uncertainty on the localization of marker

163 centroids ranges from 0.015 to 0.022 px for the three registration transformations. The corresponding

164   uncertainty on the measure of the SNR is less than 0.4 dB in the worst case.

V. RESULTS

166   The three subjects whose results are reported in this paper had respectively small breast size (cup A,

167   subject 1), medium breast size (cup B, subject 2), and large breast size (cup DD, subject 3).

168   Fig. 1a shows the two sets of markers applied to subject 3 (large breast size), whereas Fig. 1b depicts a

169   thermographic shot of the same subject showing superimposed (black lines) the Delaunay triangulation

170   used in the registration procedure.

171   Figure 2 summarizes the results relative to these subjects. For each subject we report some parameters

172   describing the signal-to-noise ratio relative to the Region Of Interest (ROI) before and after applying the

173   registration algorithm. Specifically, we report the values of the median, 25th and 75th percentiles,

174   minimum and maximum of the signal-to-noise ratios expressed in decibels. The ROI is defined as the area

175   contained within the perimeter constituted by the outer triangulation lines. Notice that this ROI is slightly

176   changing over time. However, given the small percentage of pixels entering/exiting the ROI with respect

177   to the minimum-area ROI (less than 2 %), we decided to discard these pixels and to consider the same

178   ROI for all the frames of the sequence.

179   Considering the three subjects above described, before registration, the signal-to-noise ratio median

180   ranged from 1 to 2 dB (thin line boxes), whereas, after registration, it increased up to 9 dB, thus

181   demonstrating that registration causes a decrement of the noise power due to motion artifact as high as 5-

182   6 times, depending on the subject.

VI. CONCLUSION

184   In this paper, we present a methodology to estimate the noise due to patient motion that affects an

185   infrared image sequence. In turns, the knowledge of noise power allows to estimate the signal-to-noise

186   ratio that characterizes the sequence.

187   Results herein presented demonstrate that, as long as the assumptions on which the noise model is

188　based hold, it is possible to compute the signal-to-noise ratio of a specific infrared sequence of images.

189　This is an original and important result, since it allows to assess objectively the effectiveness of different

190　registration algorithms, as well as to obtain a quantitative evaluation of the quality of an infrared sequence

191　of images.

192　　The evaluation of the ROC curves of any detector used to differentiate sequences obtained from normal

193　or pathological subjects is not possible without the knowledge of the signal-to-noise ratio of the sequence.

194　Hence, we believe this noise estimation method will crucial to fill a gap that currently limits the

195　possibility of further improving the results given by dynamic infrared imaging in early breast cancer

196　detection and, consequently, also limits its spreading in clinics.

200　　　　　　　　　　　　　　　　　REFERENCES

201　[1] K.R. Foster, "Thermographic detection of breast cancer", *IEEE Eng. Med. Biol.*, Vol. 17, Issue 6, pp.

202　　　10-14, 1998.

203　[2] M. Anbar, L. Milescu, A. Naumov, C. Brown, T. Button, C. Carty and K. AlDulaimi, "Detection of

204　　　Cancerous Breasts by Dynamic Area Telethermometry", *IEEE Eng. Med. Biol.*, Vol. 20, pp. 80-91,

205　　　2001.

206　[3] M. Anbar, C. Brown, L. Milescu, L. Babalola and L. Gentner, "The potential of dynamic area

207　　　telethermometry in assessing breast cancer", *IEEE Eng. Med. Biol.,* Vol. 19, pp. 58-62, Mar./Apr.

208　　　2000.

209　[4] T.M. Button, H.. Li, P. Fisher, R. Rosenblatt, K. Dulaimy, S. Li, B. O'Hea, M. Salvitti, V. Geronimo,

210　　　C. Geronimo, S. Jambawalikar, P. Carvelli and R. Weiss, "Dynamic infrared imaging for the

211　　　detection of malignancy", *Phys. Med. Biol.,* 49, pp. 3105-3116, 2004.

212 [5] M. Janicek, G. Demetri, M.R. Janicek, K. Shaffer, M.A. Fauci, "Dynamic Infrared Imaging of Newly

213   Diagnosed Malignant Lymphoma Compared with Gallium-67and Fluorine-18 Fluorodeoxyglucose

214   (FDG) Positron Emission Tomography", *Tech. In Cancer Res. and Treatment*, Vol. 2, Num. 6, pp.

215   571-577, 2003.

216 [6] V. Agostini, S. Delsanto, F. Molinari, M. Knaflitz, "Evaluation of feature-based registration in

217   dynamic infrared imaging for breast cancer diagnosis", Proceedings of the 28th IEEE EMBS Annual

218   International Conference, New York, USA, pp.953-956, 2006.

219 [7] A. Goshtasby, "Piecewise linear mapping functions for image registration", Pattern Recognition, vol.

220   19, pp. 459-466, 1986.

221 [8] L. Zagorchev, and A. Goshtashby, "A Comparative Study of Transformation Functions for Nonrigid

222   Image Registration", IEEE Transactions on Image Processing, vol. 15, no. 3, pp. 529-538, 2006.

223 [9] F. Aurenhammer, Voronoi diagrams—a survey of a fundamental geometric data structure, ACM

224   Computing Surveys (CSUR), vol. 23, Issue 3, pp. 345 – 405, 1991.

225

226

Figures captions

228   Fig. 1a. Picture of subject 3. Control points are represented by light-colored markers, while test points by

229   dark markers. Fig. 1b-c. Single frame extracted from the infrared sequence: Delaunay triangulation is

230   shown superimposed (Fig. 1b); Voronoi regions are shown superimposed (Fig. 1c).

231

232

233   Fig. 2. Boxplot of the signal to noise ratio (SNR) before (thin line) and after (thick line) registration for

234   three different subjects respectively with small (subject 1), medium (subject 2) and large (subject 3) breast

235   size. Each box reports the median value, percentiles (25th and 75th), minimum and maximum representing
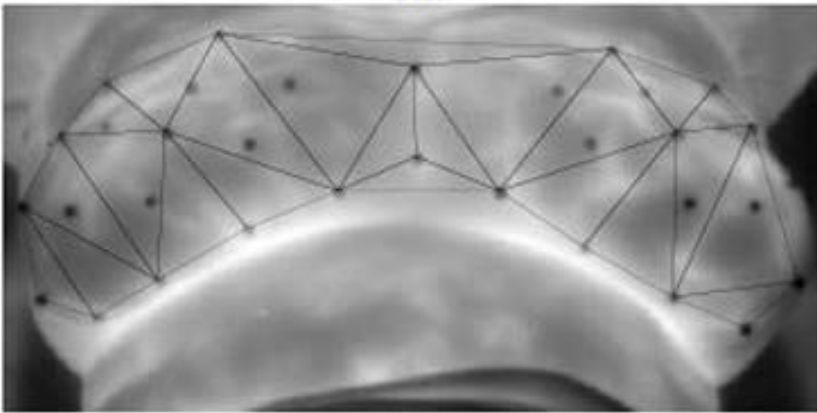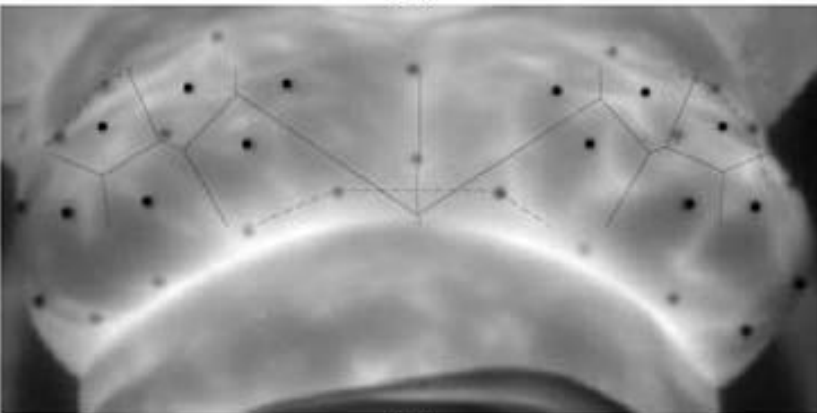
236   the SNR(x,y) distribution relative to the region of interest.

237

238   Figura 1

239

(a)

(b)

(c)

240   Figura 2